Геология и геофизика, 2018, т. 59, № 3, с. 372—385

УДК 550.382.3+553.94+510

ВЛИЯНИЕ ЛОКАЛЬНЫХ НАПРЯЖЕНИЙ И ТРЕЩИН НА ПРОНИЦАЕМОСТЬ УГОЛЬНОГО ПЛАСТА В БЛОКЕ ЛИНЬФЭНЬ

(*юго-восточная часть бассейна Ордос, Китай*)

Линьлинь Ван[a, b], Бо Цзян[a], Цзилинь Ван[a], Цзяо Ван[a], Чжэнхуй Цюй[a]

[a] *Ministry of Education Key Laboratory of CBM Resources and Reservoir Formation Process, School of Resources and Geosciences, China University of Mining and Technology, Xuzhou 221116, China*

[b] *Low Carbon Energy Institute (Key Laboratory of Coal-based CO_2 Capture and Geological Storage of Jiangsu Province), China University of Mining and Technology, Xuzhou 221008, China*

Влияние локальных напряжений и трещин на проницаемость угольного пласта зависит от их взаимной ориентации. Ориентация локальных напряжений в блоке Линьфэнь в юго-восточной части бассейна Ордос определялась систематическими измерениями трещин в лессах. Величины локальных напряжений рассчитывались по данным каротажа и гидравлического разрыва пласта. Были изучены ориентации трещин в угольном пласте № 5 и распределение плотностей перекрывающего его слоя песчаника. Результаты показывают, что максимальное горизонтальное напряжение имеет северо-восточное направление, почти параллельное преобладающей ориентации трещин в угольном пласте, что способствует их открытию. Минимальное горизонтальное напряжение, ориентированное перпендикулярно преобладающей ориентации трещин, провоцирует их закрытие. Угольный пласт № 5 характеризуется напряжениями $\sigma_v > \sigma_H > \sigma_h$, что способствует открытию субвертикальных трещин и увеличению проницаемости пласта. Очевидно, что проницаемость угольного пласта № 5 возрастает с увеличением эффективного вертикального напряжения и эффективного максимального горизонтального напряжения. Кроме того, установлена четкая экспоненциальная зависимость проницаемости угольного пласта № 5 от плотности концентрации трещин преобладающей ориентации. Поэтому трещины с преобладающей ориентацией 45° главным образом способствуют повышению проницаемости угольного пласта № 5 в блоке Линьфэнь. Многомерный анализ показывает четкие экспоненциальные зависимости между проницаемостью, плотностью концентрации трещин преобладающей ориентации и эффективным напряжением в угольном пласте № 5.

Локальное напряжение, трещина, проницаемость, угольный пласт, бассейн Ордос

EFFECTS OF IN-SITU STRESS AND JOINT ON PERMEABILITY OF THE COAL BED IN LINFEN BLOCK, SOUTHEASTERN ORDOS BASIN, CHINA

Linlin Wang, Bo Jiang , Jilin Wang, Jiyao Wang, Zhenghui Qu

Effects of in-situ stress and joint on permeability of the coal bed depend on orientation relationships between in-situ stress and joint. In-situ stress orientations of Linfen block of southeastern Ordos Basin were determined by systematical measurements of the loess joints. In-situ stress magnitudes were calculated based on well logging and hydraulic fracturing data. Joint orientations of the No.5 coal bed and density distributions of the overlying sandstone bed were investigated. The results show that the NE-oriented maximum horizontal principal stress, approximately parallel to the predominant joint orientation of the coal bed, is favorable to the openness of the predominant joints. The minimum horizontal principal stress, with its orientation perpendicular to the predominant joint orientation, tends to induce the closure of the predominant joints. The stress state of No.5 coal bed is $\sigma_v > \sigma_H > \sigma_h$, which is favorable for the openness of subvertical joints and an increase in permeability. The permeability of No. 5 coal bed increases obviously with increasing effective vertical stress and effective horizontal maximum stress and decreases with increasing effective horizontal minimum stress. Besides, the permeability of No. 5 coal bed exhibits a good exponential relationship with the density of predominant joint set. Therefore, predominant joints with the orientation of 45° mainly contribute to increases in the permeability of the No. 5 coal bed in Linfen block. Multidimensional analysis show good exponential relationships among the permeability, predominant joint density, and effective stress of the No.5 coal bed.

In-situ stress, joint, permeability, coal bed, Ordos Basin

1. INTRODUCTION

Permeability of the coal reservoir greatly affects the productivity and commercial exploitation of coalbed methane (CBM). Influencing factors of permeability, i.e. coal rank, macerals, burial depth, coal texture, in-situ stress, fracture (joint and cleat) and etc., have been investigated in previous studies (Flores, 1998; Ye et al.,

✉e–mail: jiangbo@cumt.edu.cn

DOI: 10.15372/GiG20180308

1999; Fu et al., 2001; Groshong, 2009). It is thought that the permeability of the coal bed is composed of matrix permeability and fracture permeability; the matrix permeability, generally far lower than the fracture permeability, could be ignored (close, 1993). Therefore, the permeability of the coal bed mainly depends on the number, scale, connectivity and openness of the fracture. Levine (1996) revealed that permeability of the coal bed is inversely proportional to fracture spacing and proportional to fracture width.

Permeability of the coal bed is also closely related to the in-situ stress. Previous studies have focused on relationships between the permeability and the stress. It is indicated that the permeability decreases exponentially with increasing effective stress of the coal bed during CBM production in many coal beds of United States (Mckee et al., 1988), China (Meng et al., 2011) and Australia (Enever and Henning, 1997). Permeability-stress tests of coal samples also revealed that the permeability decreases with increasing stress (He et al., 2000). However, the relationship between permeability and stress is affected by the orientations of stress and fracture (Seidle et al., 1992; Zhang et al., 2000; Liu and Rutqvist, 2010). Qin et al. (1999) and Zhang et al. (2003) revealed that when fractures strike parallel to maximum compressive stress, the increase of the principal stress difference induces the openness of fractures in the coal bed, and thereby permeability increases; While the fractures, striking perpendicular to maximum compressive stress, tend to close, and are not beneficial to the increases of permeability. Therefore, controls of stress on permeability can be achieved by changes of the openness of the fracture; fracture width is the function of stress magnitude and orientation. In order to reveal the effects of stress and fracture on the permeability, it is necessary to understand direction relationships between fracture and in-situ stress.

Therefore, the Linfen block of southeastern Ordos basin is chosen as the study area to achieve three primary goals: (1) to study in-situ stress characteristics (stress orientation, horizontal and vertical distributions of stress magnitude); (2) to study joint orientation of the coal bed and density characteristics of the overlying sandstone bed; (3) to reveal controls of stress and joint on permeability based on the relationship between orientations of stress and joint. Research results will provide a basis for prediction of high-permeability block in CBM production areas with well-developed joints.

2. GEOLOGICAL SETTINGS

Linfen block is located in the southeast margin of the Ordos basin, and belongs to the south part of Jinxi fold belt (Fig.1). The study area is an overall NE-striking, NW-inclined monocline, with some local secondary

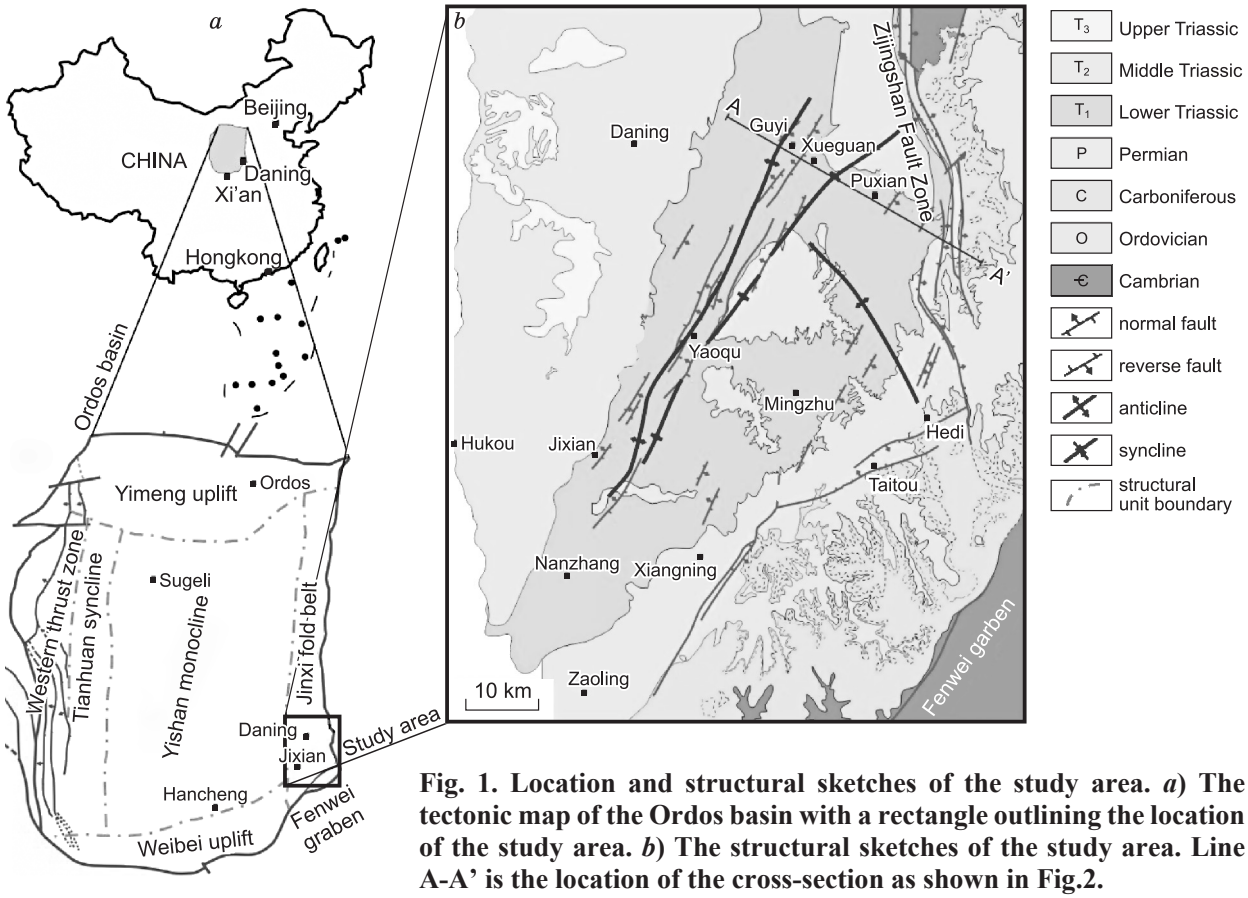

Fig. 1. Location and structural sketches of the study area. *a*) The tectonic map of the Ordos basin with a rectangle outlining the location of the study area. *b*) The structural sketches of the study area. Line A-A' is the location of the cross-section as shown in Fig.2.

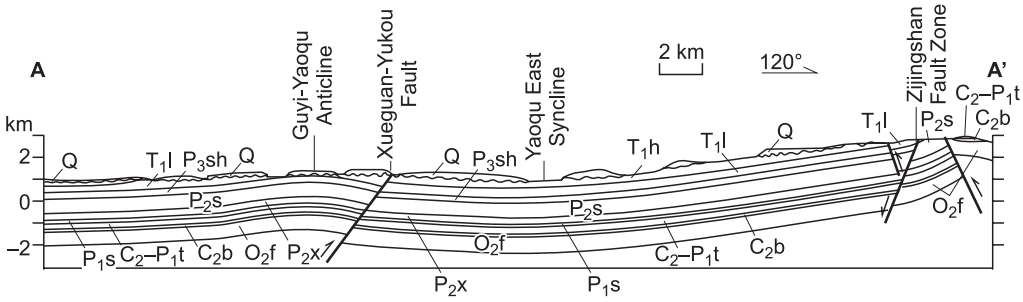

Fig. 2. Structural section of A-A' in the study area (see Fig. 1 for the section location).

Q (Quaternary), T_1h (Lower Triassic Heshanggou formation), T_1l (Lower Triassic Liujiagou formation), P_3sh (Upper Permain Shiqianfeng formation), P_2s (Middle Permain Upper Shihezi formation), P_2x (Middle Permain Lower Shihezi formation), P_1s (Lower Permain Shanxi formation), C_2-P_1t (Upper Carboniferous–Lower Permain Taiyuan formation), C_2b (Upper Carboniferous Benxi formation).

faults and folds (Fig.2). The structural lines are mostly NE-NEE-oriented, such as Guyi-Yaoqu fault and fold belt and Hedi-Taitou fault belt, excluding the nearly NS-striking Zijingshan fault zone. The study area is subjected to multi-phase compressions of the Indosin, Yanshan and Himalayan. The NW-SE-oriented Yanshanian compression is the key tectonic activity, inducing the formations of NE-striking structures (Wang et al., 2013).

The strata of this study area mainly consist of formations of Cambrian, Ordovician, Carboniferous, Permian and Triassic (Figs. 1 and 2). The Carboniferous-Permian coal-bearing strata are exposed near the Zijingshan fault zone and Hedi-Taitou fault belts, and eroded away in the northeast and southeast corners, due to tectonic compression and uplift. The No.5 coal bed of Shanxi formation, as main mined coal bed, with large thickness, intermediate coal rank and stable distribution, is considered as one target formation favorable for CBM enrichment (Chen et al., 2009).

3. IN-SITU STRESS CHARACTERISTICS

3.1. Orientation of in-situ stress

The conjugated shear joints in the Quarternary loess are considered as the result of tectonic stress, as in the other types of rocks (Wang, 2003). The acute angle bisector of conjugate shear joint indicates the direction of the maximum principal stress. The conjugated shear joints are well developed in the study area, and thereby it is possible to determine in-situ stress directions by systematical joint measurements in the loess.

The orientations of shear joints developed in the loess were measured at 8 sites, and orientations of 216 joints were collected. The shear joints in the loess are characterized by the smooth joint plane and the dipping angle of nearly 90° as shown in Fig. 3. The sub-vertical to vertical conjugated shear joint indicates that the orientation of the maximum principal stress is sub-horizontally oriented. Projections of measured shear joints indicate that the angles between conjugate shear joints range from 65° to 80°. The orientations of the maximum principal stress, σ_1, change from NNE in the north (S1 and S2) to NE (S3, S4 and S5) in the center, and then to NEE in the south (S6 and S7). The stress trajectory exhibits curved bending to SE (Fig. 3). Those coincide with previous results of the orientation of regional in-situ stress by other researchers. Through the focal mechanism solution of seismic data, Wan (2004) found that Mainland China exhibited horizontal in-situ stress orientation, and the orientation of maximum principal stress of the Ordos basin was NEE. Based on underground in-situ stress measurement data, Kang (2009) proposed that the maximum compressive stress orientation of regional in-situ stress struck NE-SW.

3.2. In-situ stress calculation

3.2.1 In-situ stress model

The vertical principal stress, a result of the overburden, varies with the strata density and buried depth, and can be calculated applying rock density logging data as shown in Eq. (1).

$$\sigma_v = \int_0^H \rho(h) g dh \tag{1}$$

Where σv is the vertical principal stress, MPa, H represents the burial depth of strata, m, g denotes the acceleration of gravity, 9.8m·s^2, and $\rho(h)$ is the density function varying with strata depth, g/cm^3.

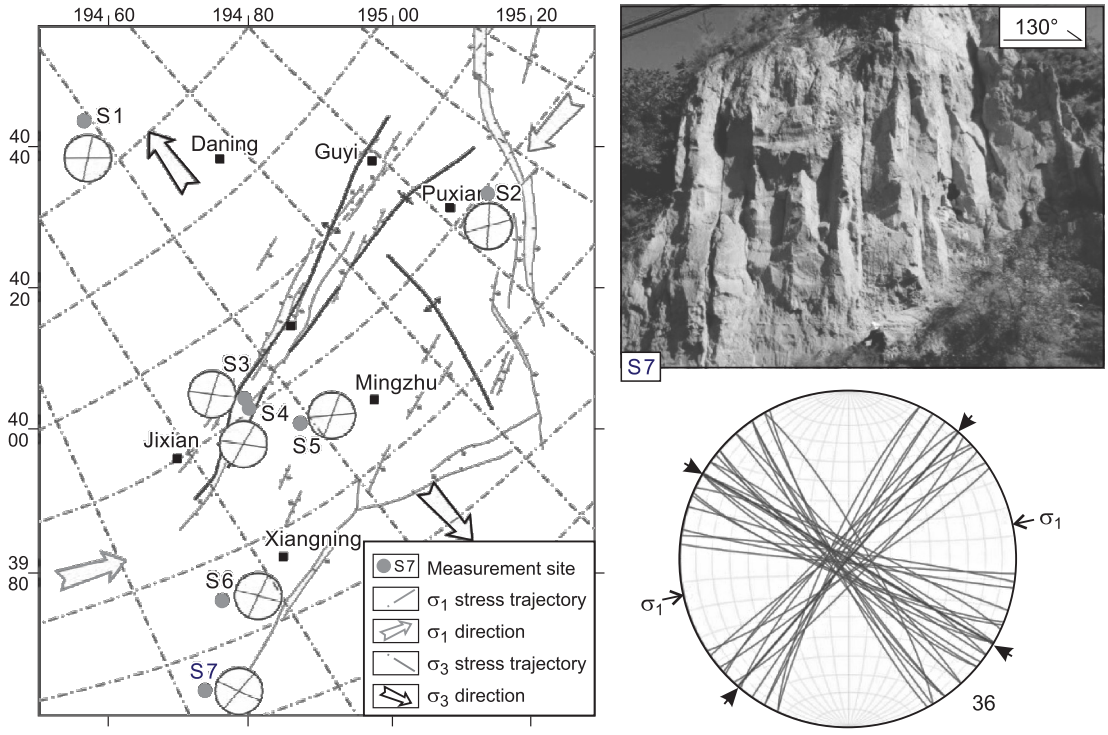

Fig. 3. Directions of Loess joint and in-situ stress trajectories in the study area

The other two principal stresses are located in the horizontal plane. The Anderson model added by tectonic stress, described as Eqs. (2) and (3), is used in the present study (Ma and Sun, 2002).

$$\sigma_H - \alpha P_P = \frac{\nu}{1-\nu}\left(\sigma_v - \alpha P_P\right) + S_{tH} \tag{2}$$

$$\sigma_h - \alpha P_P = \frac{\nu}{1-\nu}\left(\sigma_v - \alpha P_P\right) + S_{th} \tag{3}$$

Where σ_H and σ_h are the maximum and minimum horizontal principal stress, respectively, MPa, v is the Poisson's ratio, P_p is the pore pressure, MPa, α is the pore compressibility coefficient, S_{tH} and S_{th} are the maximum and minimum horizontal tectonic stress, respectively, MPa.

3.2.2 Parameter calculation

In order to calculate the in-situ stress employing above stress calculation models, the involving parameters, such as the Poisson's ratio, v, pore compressibility coefficient, α, and strata pore pressures, P_p, horizontal tectonic stresses, S_{th} and S_{tH}, should be obtained.

(1) Poisson's ratio, v

The Poisson's ration can be obtained employing acoustic wave time difference and density logging data. The empirical relation between time differences of the S-wave and P-wave can be demonstrated by (Yang, et al., 2008)

$$\Delta t_s = \frac{\Delta t_p}{1 - 1.15\left[\dfrac{(1/\rho) + (1/\rho)^3}{e^{(1/\rho)}}\right]^{1.5}} \tag{4}$$

The Poisson's ratio is written by (Zhang and Lin, 2001)

$$\nu = \frac{1}{2}\left|\frac{\Delta t_s^2 - 2\Delta t_p^2}{\Delta t_s^2 - \Delta t_p^2}\right| \tag{5}$$

where ρ is the volume density of rock, g/cm^3, Δt_s is the S-wave time difference, μs/m, and Δt_p is the P-wave time difference, μs/m.

(2) Pore compressibility coefficient, α

α is the Biot poroelastic parameter (Biot and Willis, 1957), and is calculated by Eqs.(6)-(8).

$$\alpha = 1 - \frac{C_{ma}}{C_b} \tag{6}$$

$$C_{ma} = \frac{1}{\rho_{ma} \dfrac{3\Delta t_{mas}^2 - 4\Delta t_{map}^2}{3\Delta t_{mas}^2 \Delta t_{map}^2} \times 10^9} \tag{7}$$

$$C_b = \frac{1}{K} = \frac{1}{\rho \dfrac{3\Delta t_s^2 - 4\Delta t_p^2}{3\Delta t_s^2 \Delta t_p^2} \times 10^9} \tag{8}$$

Where C_{ma} is rock matrix compressibility, C_b is rock bulk compressibility, ρ_{ma} is rock matrix density, g/cm^3, Δt_{mas} is the S-wave time difference of the rock matrix, μs/m, Δt_{map} is the P-wave time difference of the rock matrix, μs/m.

(3) Prediction of pore pressure based on Eaton's approach

Based on the Eaton's method (Kumar et al., 2006), the prediction model of pore pressure, P_p, is described as

$$P_p = P_0 - (P_0 - P_n)(\Delta t_n / \Delta t)^c \tag{9}$$

where P_0, P_n are overburden pressure and strata hydrostatic pressure, MPa, respectively, Δt and Δt_n are measured acoustic time difference and the acoustic time difference at the normal compaction trend line at a certain depth, respectively, μs/*ft*, c is the Eaton constant. In order to obtain P_p according to Eq. (9), Δt_n and c should be obtained firstly.

In the single log coordinate system, the acoustic time difference at the normal compaction section for mudstone decreases linearly with increasing depth (Kumar et al., 2006). Because Eaton's approach was established based on mudstone, more than 2-m-thick mudstone intervals of four CBM wells were selected (Fig. 4, Table 1). It is clearly seen in Fig. 4 that the relationship between the acoustic time difference and depth, i.e. the equation of normal compaction trend line, is described as

$$\ln(\Delta t_n) = -1.4614 \times 10^{-3} H + 6.5731 \tag{10}$$

The Eaton constant can be written by

$$c = \frac{\ln\left[(P_0 - P_p)/(P_0 - P_n)\right]}{\ln(\Delta t_n / \Delta t)} \tag{11}$$

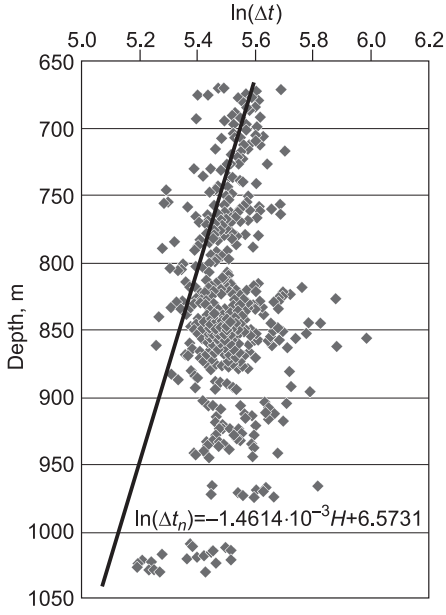

According to strata pressure data (Table 1) and Eq. (11), Eaton constants of four CBM wells were calculated (Table 1) and the average value of c is equal to -0.5538.

Therefore, the pore pressure of the study area can be finally obtained as shown in Eq. (12).

$$P_p = P_0 - (P_0 - P_n)\left(\frac{e^{-1.4614H\times10^{-3}+6.5731}}{\Delta t}\right)^{-0.5538} \tag{12}$$

(4) Maximum and minimum horizontal tectonic stress, S_{tH} and S_{th}

Hydraulic fracture theories and tests indicate that the minimum horizontal principal stress, σ_h, is synonymous with closure pressure as shown in Eq.(13). Relationships between maximum and minimum horizontal principal stress are demonstrated by Eqs.(14) & (15).

Fig. 4 The normal compaction trend line of coal-bearing strata

Table 1. **Calculation results of Eaton constant (Parameters in the table are the same as above)**

Well	H	P_0(MPa)	P^*_p(MPa)	P_n(MPa)	Δt_n	Δt	c
J15	924.47	21.65	5.08	7.92	185.2840	208.61	–1.5878
J9	1056.36	26.92	7.53	7.80	152.8002	181.78	–0.0814
J17	990.86	24.40	6.19	7.75	168.1494	190.64	–0.7118
J18	996.56	23.69	6.30	5.60	166.7545	211.78	0.1656

$$\sigma_h = P_C \tag{13}$$

$$\sigma_H = 3\sigma_h - \alpha P_P - P_b + S_t \tag{14}$$

$$S_t = P_b - P_r \tag{15}$$

where P_C is the closure pressure, MPa, P_b is breakdown pressure of the coal, MPa, P_r is the fracture reopening pressure, MPa, S_t is the tensile strength of the coal, MPa.

Based on hydraulic fracturing data of the coal bed, the in-situ stress models in Eqs. (2) and (3) are substituted into Eqs.(13)-(15) to obtain S_{tH} and S_{th}. Finally, σ_v, σ_H and σ_h can be obtained through substituting required parameters, calculated by Eqs. (4)-(15), to Eqs. (1)-(3).

3.2.3. Calculation results

(1) In-situ stress profile of single well

Changes of principal stresses with depths of 24 CBM wells were derived based on the above in-situ stress calculation model and corresponding parameter predictions. Principal stress characteristics of well J13 are shown in Fig. 5.

The vertical principal stress, due to the cumulative weight of overlying strata, presents obviously linear relationship with the buried depth. Meanwhile, horizontal principal stresses exhibit an overall linear increase with increasing depth. However, increase amplitudes of horizontal principal stresses are smaller than those of vertical principal stresses. Besides, variations of horizontal principal stresses, related to the stratum lithology, exhibit the zigzag in the vertical direction. At the shallower strata, the maximum horizontal principal stress is generally larger than the vertical one. Therefore, the initial maximum principal stress is the horizontal principal stress. However, when the buried depth exceeds a certain value, the vertical principal stress transforms to the maximum principal stress due to its larger increase gradient. It is obviously observed from well J13 that when the buried depth is larger than 720 m, the vertical principal stress exceeds the horizontal principal stresses and thus becomes the maximum principal stress.

(2) In-situ stress characteristics of No. 5 coal bed

Based on principal stress profiles of 24 CBM wells and buried depths of No. 5 coal bed, three principal stresses of No. 5 coal bed at 24 wells can be obtained. Therefore, horizontal distributions of principal stresses of No. 5 coal bed in the study area can be acquired using the linear extrapolation method (Figs. 6-8). It should be noted that in-situ stress calculation model and corresponding parameters calculations are obtained based on the rock. The coal, as one type of extremely soft rock, presents large differences in the lithology and the acoustic wave time difference, which induces abnormal increases in horizontal principal stresses of the coal bed. For example, horizontal principal stresses of coal beds of No. 5 and No. 8 at well

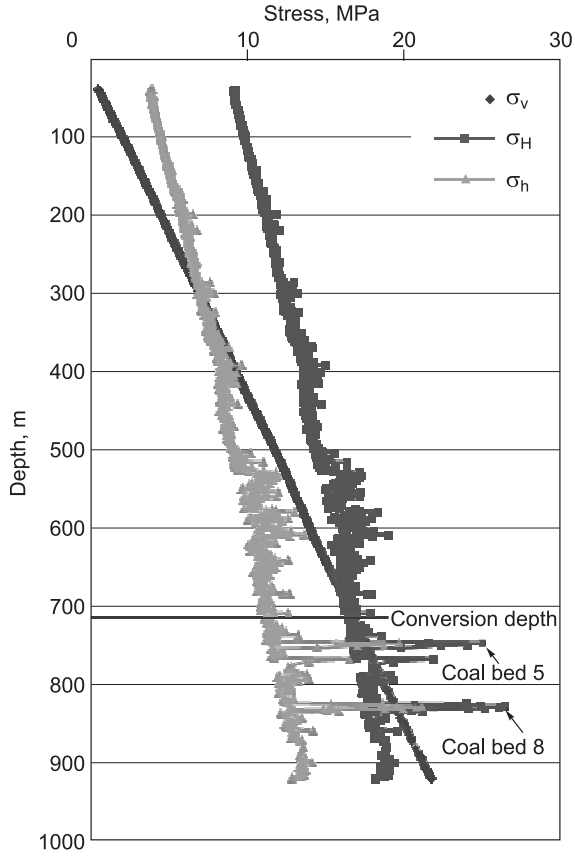

Fig. 5. In-situ stress profile of well J13

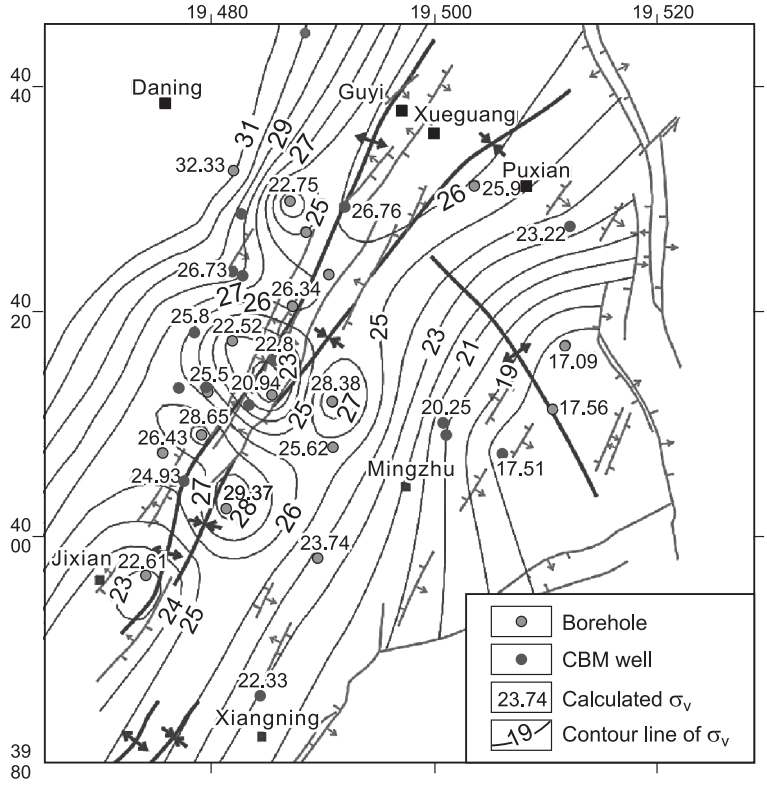

Fig. 6. Horizontal distributions of the vertical principal stress of No. 5 coal bed

J13 are much larger than vertical principal stresses and exhibit obvious zigzags, which do not agree with overall variation trends of three principal stresses in the vertical direction. Therefore, average values of horizontal principal stresses of hard roof and floor rocks of the coal bed are regarded as horizontal principal stresses of the coal bed.

The vertical principal stress, maximum and minimum horizontal principal stresses of No. 5 coal bed in the study area vary in ranges of 17-32 MPa, 17-28 MPa and 13-18 MPa, respectively (Figs. 6-8). It is obviously observed from in-situ stress profiles of the single well that vertical and horizontal principal stresses both increase with increasing buried depth (Fig. 5). The buried depth of strata, obviously affected by the structure deformation, exhibits an overall increasing trend from east to west, with local complex variations in Guyi-Yaoqu fault and fold belts (Fig. 2). Therefore, three principal stresses show the similar horizontal variations as burial depth of the coal bed. It is clearly seen from Figs. 6-8 that in the study area, three principal stresses show gradual increases with increasing buried depth from the southeastern margin towards northwest to Yaoqu east syncline, and thereby the Yaoqu east syncline axis exhibits the high in-situ stress region. However, near the Guyi-Yaoqu anticline, the coal bed with decreased buried depth shows the strip of low principal stresses attributed to the strata uplift. Meanwhile, Guyi-Yaoqu fault and fold presents complex stress variations along the structural line direction. Local increases or decreases in in-situ stresses along NE-oriented structural lines, corresponding to local increases or decreases in buried depths of coal beds, reveal the complexity or heterogeneity of the tectonic deformation. The strata, towards northwest away from the Guyi-Yaoqu fault and fold belt, gradually transit to the monocline, and three principal stresses increase gradually.

(3) Conversion depth of maximum principal stress

As previously noted, the maximum horizontal principal stress at shallower strata, larger than the other two principal stresses, is regarded as

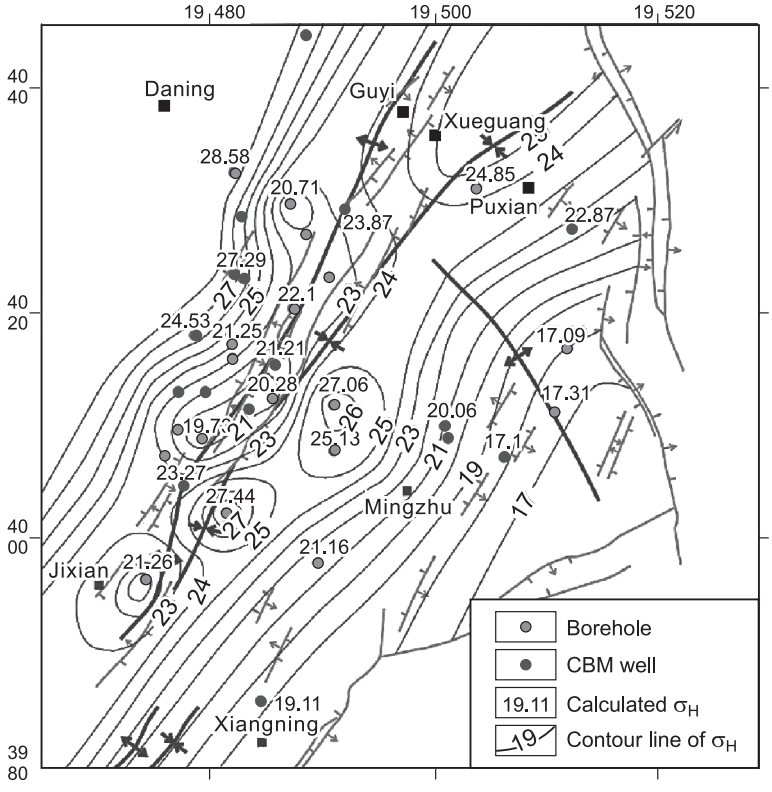

Fig. 7 Horizontal distributions of maximum horizontal principal stress of No. 5 coal bed

Fig. 8. Horizontal distributions of minimum horizontal principal stress of No. 5 coal bed

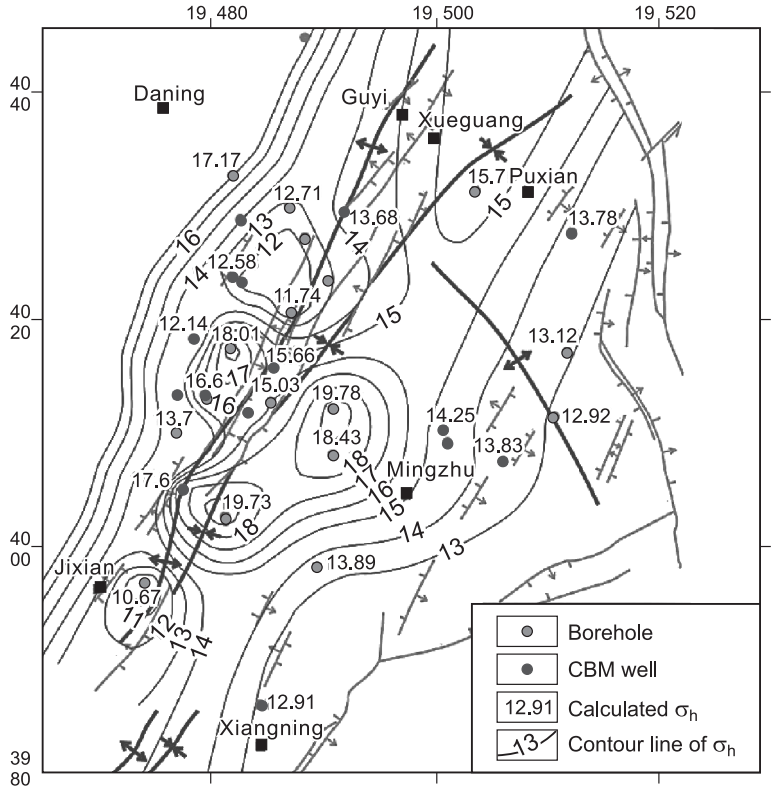

the maximum principal stress. At a critical depth, the vertical principal stress is equal to the horizontal maximum principal stress due to its large increase gradient. As the buried depth exceeds the critical value, the vertical principal stress becomes the maximum principal stress. Therefore, the critical depth is regarded as the conversion depth of maximum principal stress. The conversion depth of 24 wells can be obtained according to vertical distributions of principal stresses. The linear interpolation method is employed to obtain the horizontal distribution of conversion depth as shown in Fig. 9. The conversion depth of maximum principal stress, mainly ranging from 700 m to 1150 m, presents the overall low-high-low-high variation trend from east to west, which coincides with change laws of structurally-controlled buried depth of the coal bed. The Guyi-Yaoqu anticline exhibits the lower conversion depth of maximum principal stress, with local increases in the conversion depth along the anticline axis, which reveals the complexity and heterogeneity of tectonic deformation. According to buried depths of No. 5 coal bed and maximum principal stress conversion depths of 24 wells, it is found that the buried depth of No. 5 coal bed is larger than the maximum principal stress conversion depth, and the difference between two depths ranges approximately from 26.2 m to 593.4 m. That indicates No. 5 coal bed is located below the conversion depth of maximum principal stress, and the maximum principal stress of No. 5 coal bed is the vertical principal stress.

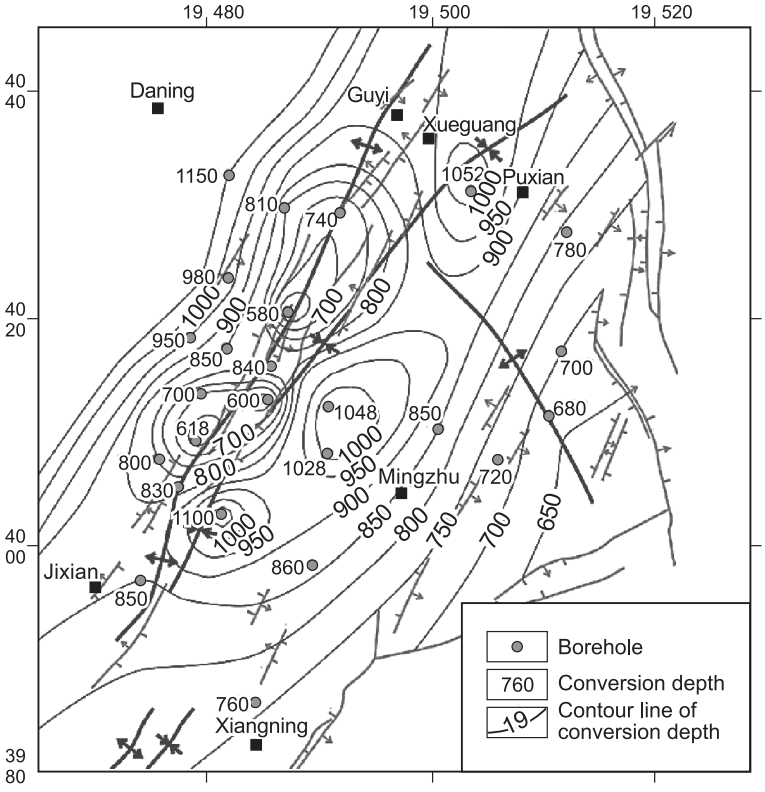

Fig. 9. Horizontal distributions of the conversion depth of maximum principal stress in the study area

4. JOINT DEVELOPMENT CHARACTERISTICS

4.1. Joint orientation

The coal-bearing strata of Carboniferous-Permian are exposed at the southeastern edge of the study area. Most parts of the study area, covered by thick Triassic strata, does not present coal seam outcrops. Therefore, coal mines are mainly located in the southeastern edge with shallow coal seams. 232 joints of coal beds and 516 joints of rock beds are measured in five coal and rock outcrops (Fig. 10). Meanwhile, 40 coal bed joints are measured in two underground coal

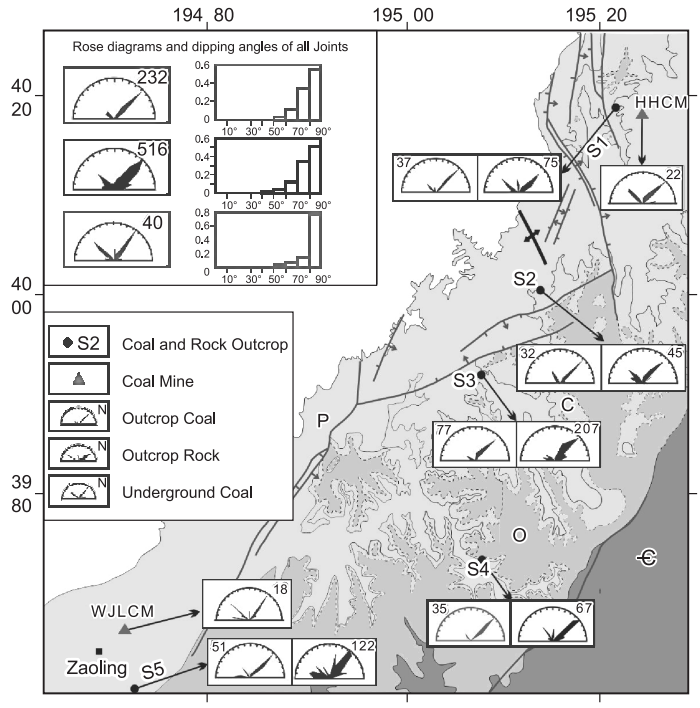

Fig. 10. Joint orientation characteristics of outcrop coal and rock beds and underground coal beds

mines (Hengsheng and Wangjialing coal mines). However, joint data of underground rock beds cannot be obtained because rock beds are not well exposed in underground coal mines. It is obviously observed from Fig. 10 that four sub-vertical joint sets, with dip angles ranging from 70° to 90°, are well developed in coal and rock outcrops and underground coal beds. The 45°-striking joint set is the most dominant, followed by the 140°-striking joint set; nearly EW- and NS- striking joints locally occurs. Therefore, joint occurrences of coal and rock outcrops, and underground coal beds, are basically consistent.

4.2. Joint density

Due to few coal bed outcrops in the study area, it is difficult to directly obtain horizontal distribution characteristics of joint density of the coal bed. Previous studies demonstrate that underground rock beds have the same relative variations of density as those in outcrop rock beds at the same site (Wheeler et al., 1978; Dixon et al., 1979). Therefore, the joint density data of outcrop rock beds can be used to study the control of joint development of underground coal beds on the permeability. The joint density of the rock bed depends on thickness of the rock bed (Davis et al., 2011). Therefore, the well-developed sandstone bed with the thickness of 20 cm in the study area is chosen to measure the joint density of outcrops and thereby to draw the horizontal distribution of joint density by linear extrapolation (Fig. 11). The joint density of the 20-cm thick sandstone bed mainly ranges 4-14 per meter. The joint density is obviously controlled by the structure, and exhibits a gradual increase near the fault and fold belt. The joint density is the largest in southeastern fault zones, followed by the Guyi-Yaoqu fault and fold belt. Structurally undeveloped area has the low joint density, i.e. generally smaller than 8 per meter.

5. EFFECTS OF IN-SITU STRESS AND JOINT ON PERMEABILITY OF NO. 5 COAL BED

5.1. Determination of permeability

The permeability of coal reservoir can be determined employing methods of determining conventional oil and gas reservoir permeability, such as core laboratory test, reservoir simulation, geophysical methods (including seismic and logging methods) and well test (Mohammadi et al., 2013). However, only well test can demonstrate the in-situ permeability of coal reservoir under the fluid flow state. The routine well test methods consist of drill stem test, slug flowing test, injection pressure drop test and water jug test. Attributed to the generally low pressure reservoir and permeability of coal beds in China, the injection

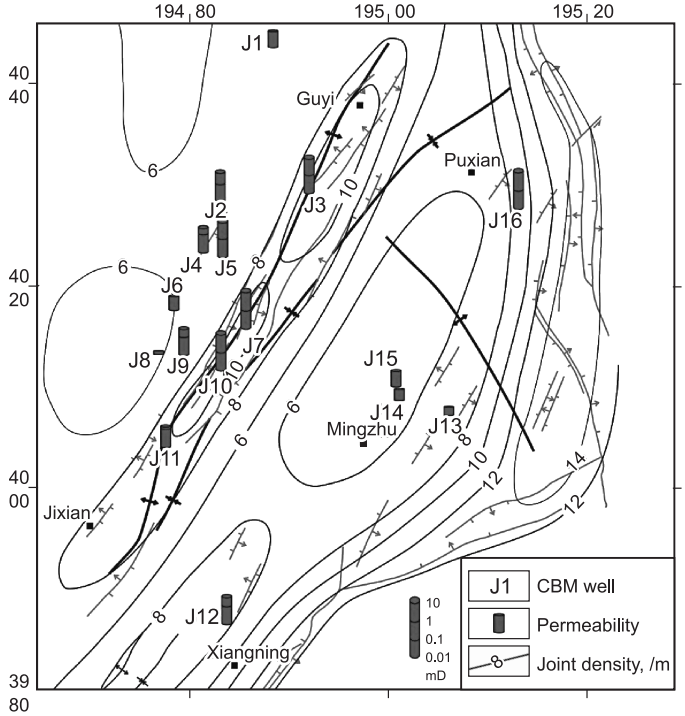

Fig. 11. Horizontal distributions of density of dominant joint set of No. 5 coal bed (Wang et al., 2016)

Table 2. **Permeability data gained from well testing of No.5 coal bed**

Well	Depth (m)	Permeability (mD)	Well	Depth (m)	Permeability (mD)	Well	Depth (m)	Permeability (mD)
J1	1124	0.088	J7	923.2	1.011	J13	746.2	0.028
J2	1011.2	0.49	J8	950	0.0162	J14	866.4	0.0478
J3	1059	0.75	J9	996	0.283	J15	826.4	0.0839
J4	1178.4	0.288	J10	880	0.98	J16	1000	2.45
J5	967	0.81	J11	998	0.141			
J6	1078.4	0.065	J12	900.1	0.3049			

pressure drop test method, as the single well transient pressure test method, is widely employed (Chen and Lian, 2003). The testing procedure is as follows: at first, put the testing tools (testing string, packer, pressure gauge, etc.) into the well; afterwards, inject water into the well for certain time with the stable displacement and injection pressure lower than the fracture pressure of coal reservoir; then shut in when the pressure distribution region higher than initial reservoir pressure is produced surrounding the wellbore; finally the pressure surrounding the wellbore is gradually equal to initial reservoir pressure. Bottom-hole pressure can be recorded by the pressure gauge during injection and shut in, and bottom-hole pressure-time curve can be acquired, which is used for calculations of permeability, reservoir pressure and fracture pressure.

The injection pressure drop test method was employed to obtain permeability of 16 wells of No. 5 coal bed as shown in Table 2. Large differences up to three orders of magnitude can be seen among the permeability of No. 5 coal bed in Linfen block. Most of the wells show lower permeability, i.e. wells with permeability ranging from 0.1~1 mD up to 50%, and wells with permeability varying from 0.01~0.1 mD up to 37.5%, except higher permeability of wells J7 and J16 (permeability larger than 1 mD). Horizontally, the No.5 coal bed exhibits its higher permeability in structurally developed area, such as wells J7 and J10 located at Guyi-Yaoqu fault fold belt, and well J16 at the eastern fault belts. Wells far away from the structurally developed areas generally show lower permeability.

5.2. Relationships between in-situ stress and permeability

In order to investigate the relationship between in-situ stress and permeability of coal bed in Linfen area, we introduce the effective vertical stress, σ_{ve}, effective maximum horizontal stress, σ_{He}, and the effective minimum horizontal stress, σ_{he}, as written by

$$\sigma_{ve} = \sigma_v - p_p \tag{16}$$

$$\sigma_{He} = \sigma_H - p_p \tag{17}$$

$$\sigma_{he} = \sigma_h - p_p \tag{18}$$

It is observed from Fig. 12a-c that the permeability of No. 5 coal bed exhibits obvious exponential relationships with the effective stresses (σ_{ve}, σ_{He} and σ_{he}), respectively, as described by Eqs. (19-21).

$$k = 3.6415\times10^{-5} e^{0.4883\sigma_{ve}} \tag{19}$$

$$k = 6.1754\times10^{-6} e^{0.6468\sigma_{He}} \tag{20}$$

$$k = 0.8447 e^{-0.1836\sigma_{he}} \tag{21}$$

It is concluded that the permeability of No. 5 coal bed increases obviously with increasing effective vertical stress and effective horizontal maximum stress, and decreases with increasing effective horizontal minimum stress. That can be explained by stress states of No. 5 coal bed and the relationship between the joint and stress orientations.

Sub-vertical to vertical joints, with predominant strike directions of NE, are well developed in the No. 5 coal bed of the study area. As previously mentioned, the buried depth of No. 5 coal bed is larger than the conversion depth of maximum principal stress, and the stress state of No.5 coal bed is $\sigma_v > \sigma_H > \sigma_h$. Vertical joints of No. 5 coal bed are subject to the tensile stress. An increase of the vertical principal stress is favorable to the openness of joints and the increase in the permeability. Therefore, the permeability of No.5 coal bed increases with increasing effective vertical stress, and there is a good exponential relationship between the permeability and effective vertical stress.

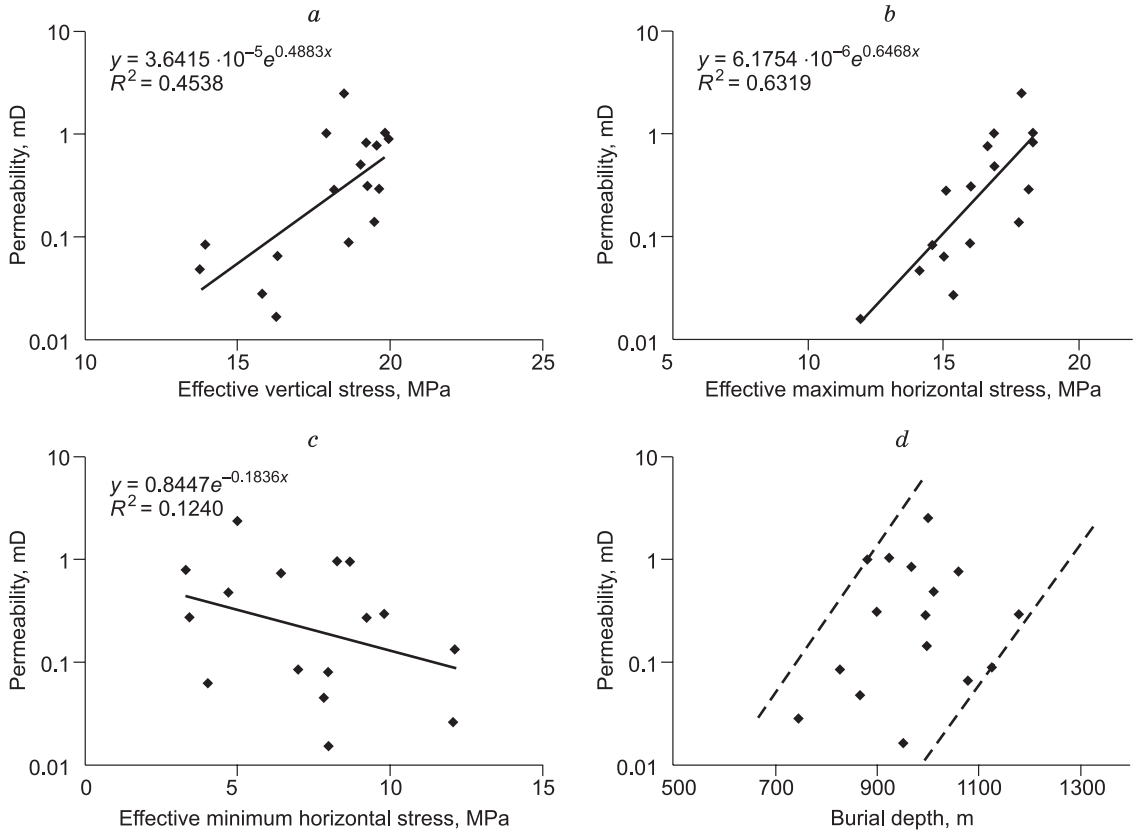

Fig. 12. Relationships between permeability and effective stress components and burial depth.

As previously mentioned, the maximum horizontal compressive stress is NE-oriented, while the predominat joint set of No. 5 coal bed strikes 55°. Therefore, the orientation of maximum horizontal compressive stress is approximately parallel to the predominant joint orientation of the coal bed. Those are favorable to the openness of the predominant joints. The permeability of No. 5 coal bed increases with increasing effective maximum horizontal compressive stress. However, the minimum horizontal compressive stress, with its orientation perpendicular to the predominant joint orientation, is not favorable to the openness of joints. Therefore, the permeability decreases gradually with increasing effective minimum horizontal stress.

Besides, the permeability of No. 5 coal bed increases with increasing buried depth (Fig. 12d). The effects of buried depth of the coal bed on the permeability are the results of complex roles of effective vertical stress, effective horizontal maximum principal stress and effective horizontal minimum principal stress. The stress states of No. 5 coal seam ($\sigma_v > \sigma_H > \sigma_h$) is favorable to the increase in permeability. Therefore, an increase in the buried depth of No. 5 coal bed induces increases in principal stresses and the permeability.

5.3. Relationships between the joint density and permeability

Horizontal distribution of the permeability of the No. 5 coal bed is obviously controlled by the structural deformation (Fig. 11). The largest joint density occurs in the superimposed area of the eastern Zijinshan fault zone and the NE-orientated faults. The corresponding permeability is also the largest up to 2.45 mD, followed by the Guyi-Yaoqu fold. However, the areas of Puxian-Mingzhu and Daning-Jixian west, far away from the structural belt and located in the stabilized area with undeveloped structure, present low joint density and permeability.

The maximum compressive stress in the study area is NE-NEE-oriented, and the predominant joint of the coal bed strikes 45°, followed by 140°. The relationship between orientations of in-situ stress and joint affects the joint openness and closure, and controls the joint width. The 45°-striking joint set is nearly parallel to the orientation of maximum horizontal compressive stress, which induces the opening of predominant joints and causes increases of the permeability of No. 5 coal bed. However, another set of joints, striking 140°, are nearly perpendicular to the orientation of maximum horizontal principal stress and tend to close, which is not favorable to the increase of permeability. It is clearly seen from Fig. 13a that the permeability of No. 5 coal bed increases

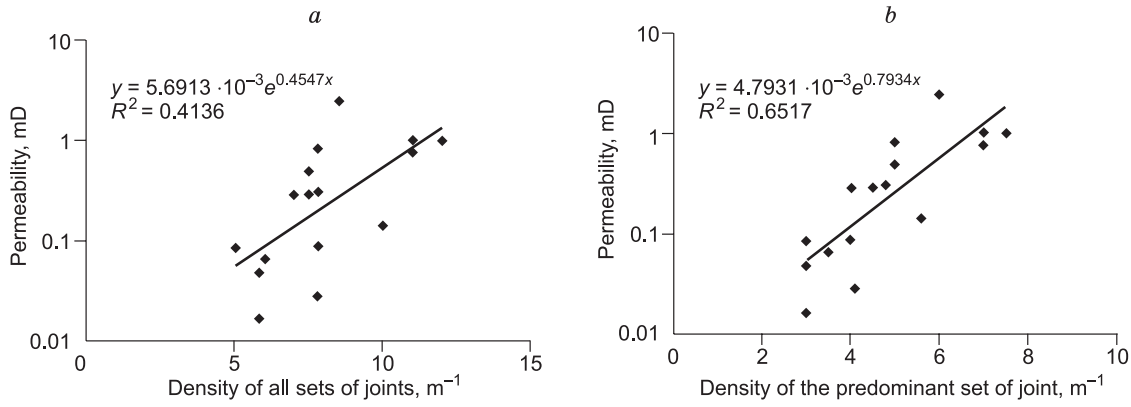

Fig. 13. Relationships between permeability and joint density of No. 5 coal bed.

with increasing total density of all sets of joints, but the data distribution is scattered. Fig. 13b shows that the permeability of No. 5 coal bed is obviously controlled by the density of predominant joint with the orientation of 45°; the joint density and permeability both increase and exhibit a good exponential relationship. Therefore, predominant joints with the orientation of 45° mainly contribute to increases of the permeability of the No. 5 coal bed in Linfen block; development characteristics of the predominant joint set affect permeability variations.

5.4. Multidimensional analysis

It is concluded in Section 5.3 that predominant joints with the orientation of 45° mainly contribute to increases of the permeability of the No. 5 coal bed in Linfen block, and there is a good exponential function relation between the permeability and predominant joint density in No. 5 coal bed. Meanwhile, the effective stress affects the joint width and thereby controls the permeability. Therefore, Eq. (22) is proposed.

$$k = ae^{bD}k_{\sigma_e} \tag{22}$$

$$\sigma_e = \sqrt{\frac{1}{2}((\sigma_v - \sigma_H)^2 + (\sigma_v - \sigma_h)^2 + (\sigma_H - \sigma_h)^2)} - p_p \tag{23}$$

where a and b are constants, D is the predominant joint density of No. 5 coal bed, /m, k_{σ_e} is the permeability change attributed to effective stress, σ_e is the effective stress.

It can be seen from Fig. 14a that the permeability and effective stress also show exponential relationship as Eq. (24).

$$k = 6.8194 \times 10^{-2} e^{0.4011\sigma_e} \tag{24}$$

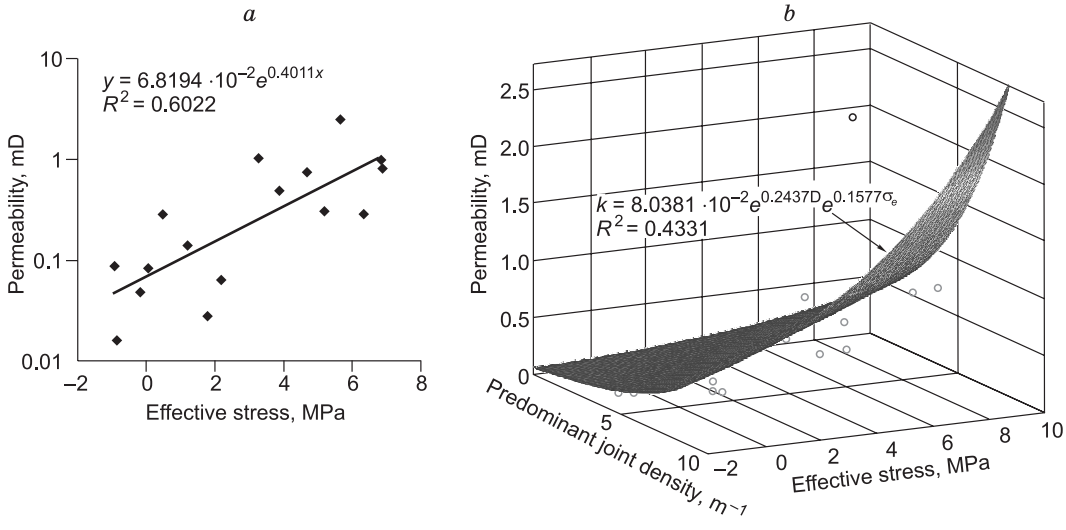

Fig. 14. Relationships between permeability and effective stress and predominant joint density.

Therefore, correlations among the permeability, predominant joint density and effective stress can be written as

$$k = ae^{bD}ce^{d\sigma_e} \tag{25}$$

where c and d are constants.

Based on the data of permeability, predominant joint density and effective stress of 16 wells of No.5 coal bed, the constants of a, b, c and d can be acquired employing nonlinear fitting methods (Fig. 14b). Finally Eq. (25) can be written as

$$k = 8.038 \times 10^{-2} e^{0.2437D} e^{0.1577\sigma_e} \tag{26}$$

6. CONCLUSIONS

The orientations of in-situ stress in the study area were determined by systematical measurements of joints developed in the loess. The in-situ stress magnitudes were calculated based on well logging and hydraulic fracturing data. The maximum principal stress, σ_1, is mainly NE-oriented. Three principal stresses exhibit an overall linear increase with increasing depth, and vertical principal stress presents the largest increase amplitude. Horizontally, three principal stresses of No. 5 coal bed show gradual increases from southeast to northwest. However, Guyi-Yaoqu fault and fold presents complex stress variations along the structural line direction due to the heterogeneity of the tectonic deformation. The conversion depth of maximum principal stress presents the overall low-high-low-high variation trend from east to west, which coincides with change laws of structurally-controlled buried depth of the coal bed. The maximum principal stress of No. 5 coal bed is the vertical principal stress.

Four sub-vertical joint sets occur in the study area, with the 45°-striking joint set as the predominant one, followed by the 140°-striking joint set and locally-developed nearly EW- and NS- striking joint sets. The joint density increases obviously near the fault and fold belt. The joint density is the largest in southeastern fault zones, followed by the Guyi-Yaoqu fault and fold belt. Structurally undeveloped area has low joint density.

The stress state of No.5 coal bed is $\sigma_v > \sigma_H > \sigma_h$, which is favorable to the openness of sub-vertical joints and the increase of the permeability. An increase in the buried depth of No. 5 coal bed induces increases in principal stresses and the permeability. Besides, the orientation of maximum horizontal principal stress, approximately parallel to the predominant joint orientation of the coal bed, is favorable to the openness of the predominant joints; the minimum horizontal principal stress, with its orientation perpendicular to the predominant joint orientation, tends to induce the closure of the predominant joint set. Therefore, the permeability of No. 5 coal bed increases obviously with increasing effective vertical stress and effective horizontal maximum stress, and decreases with increasing effective horizontal minimum stress. Based on the orientation relationship between in-situ stress and joint, the predominant joint set with the orientation of 45° is favorable to increase of the permeability. The permeability of No. 5 coal bed exhibits a good exponential relationship with the density of predominant joint set. Therefore, predominant joints with the orientation of 45° mainly contribute to increases of the permeability of the No. 5 coal bed in Linfen block. Multidimensional analysis show good exponential relationships among the permeability, predominant joint density and effective stress of the No.5 coal bed.

ACKNOWLEDGES

The research reported here was supported by National Science and Technology Major Project (Grant No. 2011ZX05034) and the Natural Science Foundation of Jiangsu Province (Grant No. BK20150177).

REFERENCES

Biot, M.A., Willis, D.G., 1957. The elastic coefficients of the theory of consolidation. J Appl. Mech. Trans. ASME 24, 594–601.

Chen, G., Zhao, Q.B., Li, W.Z., Sun, B., Sun, Q.P., Tian, W.G., 2009. Control of high permeability zone by ground stress field in Daning-Jixian area. China Coalbed Methane 6 (3), 15–20.

Chen, Z.S., Lian, Y.X., 2003. Discussion on technical problems for injection/fall-off well test in the coalbed methane well. Coal Geol. Explor. 31 (4), 23–26.

Close, J.C., 1993. Natural fracture in coal, in: Law, B.E., Rice, D.D. (Eds.), Hydrocarbons from Coal. AAPG Stud. Geol. 38, 119–132.

Davis, G.H., Reynolds, S.J., Kluth, C.F., 2011. Structural Geology of Rocks and Regions, 3rd ed. John Wiley & Sons, New York.

Dixon, J.M., 1979. Techniques and Tests for Measuring Joint Intensity. PhD dissert. West Virginia University, Morgantown.

Enever, J.R.E., Henning, A., 1997. The relationship between permeability and effective stress for Australian coal and its implications with respect to coalbed methane exploration and reservoir modeling, in: Proc. 1997 Int. Coalbed Methane Symp. The University of Alabama, Tuscaloosa, pp. 13–22.

Flores, R.M., 1998. Coalbed methane: from coal-mine outbursts to a gas resource. Int. J. Coal Geol. 35, l–4.

Fu, X.H., Qin, Y., Li, G.Z., Li, T.Z., Hu, Z., 2001. An analysis on the principal control factor of coal reservoir permeability in central and southern Qinshui basin, Shanxi. J. Geomech. 7 (1), 45–52.

Groshong, Jr. R.H., Pashin, J.C., Mcintyre, M.R., 2009. Structural controls on fractured coal reservoirs in the southern Appalachian Black Warrior foreland basin. J. Struct. Geol. 31, 874–886.

He, W.G., Tang, S.H., Xie X.D., 2000. Effect of in-situ stress on coalbed permeability. J. Liaoning Tech. Univ. (Nat. Sci.). 19 (4), 353–355.

Kang, H.P., Lin, J., Yan, L.X., Zhang, X., Wu, Y.Z., Si, L.P., 2009. Study on characteristics of underground in-situ stress distribution in Shanxi coal mining fields. Chinese J. Geophys. 52 (7), 1782–1792.

Kumar, K.M., Ferguson, R.J., Ebrom, D., Heppard, P., 2006. Pore pressure prediction using an Eaton's approach for *PS*-waves, in: SEG Tech. Prog. Expanded Abstracts 2006, pp. 1550–1554.

Levine, J.R., 1996. Model study of the influence of matrix shrinkage on absolute permeability of coalbed reservoirs. Geol. Soc. London Spec. Publ. 109, 197–212.

Liu, H.H., Rutqvist, J., 2010. A new coal-permeability model: internal swelling stress and fracture–matrix interaction. Transport Porous Med. 82 (1), 157–171.

Ma, J.H., Sun, J.M., 2002. Calculation of formation stress using logging data. Well Logging Tech. 26 (4), 347–351.

Mckee, C.R., Bumb, A.C., Koenig, R.A., 1988. Stress-dependent permeability and porosity of coal and other geologic formations. Soc. Petrol. Eng. Form. Eval. 3 (1), 81–91.

Meng, Z.P., Zhang, J.C., Wang, R., 2011. In-situ stress, pore pressure and stress-dependent permeability in the Southern Qinshui Basin. Int. J. Rock Mech. Min. 48, 122–131.

Mohammadi, H., Sedaghat, M.H., Manshad, A.K., 2013. Parametric investigation of well testing analysis in low permeability gas condensate reservoirs. J. Nat. Gas Sci. Eng. 14, 17–28.

Qin, Y., Zhang, D.M., Fu, X.H., Lin, D.Y., Ye, J.P., Xu, Z.B., 1999. A discussion on correlation of modern tectonic stress field to physical properties of coal reservoirs in central and southern Qinshui Basin. Geol. Rev. 45 (6), 576–583.

Seidle, J.P., Jeansonne, M.W., Erickson D.J., 1992. Application of matchstick geometry to stress dependent permeability in coals. SPE, 24361.

Wan, T.F., 2004. The Tectonics Outline of China. Geological Publishing House, Beijing.

Wang, L.L., Jiang, B., Qu, Z.H., 2013. Structural control on gas content distribution in eastern margin of Ordos basin. Coal Geol. Explor. 41 (1), 14–19.

Wang, L.L., Jiang, B., Wang, J.L., Qu, Z.H., Chen, R., 2016. Structural controls on joint development in the southeastern margin of the Ordos basin. Arab. J. Geosci. 9, 352.

Wang, L.M., 2003. Loess Dynamics. Seismological Press, Beijing.

Wheeler, R.L., 1978. Cross-strike structural discontinuities: Possible exploration tool in detached forelands. Geol. Soc. Am. Abstracts with Programs 10 (4), 201.

Yang, X.J., Zhang, M., Yan, X.Z., 2008. Study on rock elasticity parameters based on acoustic logging information. Petrol. Geol. Eng. 22 (4), 39–42.

Ye, J.P., Qin, Y., Lin, D.Y., 1999. Coalbed Methane Resources of China. China University of Mining and Technology Press, Xuzhou.

Zhang, J., Bai, M., Roegiers, J.C., Wang, J., Liu, T., 2000. Experimental determination of stress–permeability relationship, in: Proc. Fourth North American Rock Mechanics Symp., Seattle. Balkema, Rotterdam, pp. 817–822.

Zhang, J., Lin, S.W., 2001. Analysis of formation elastic characteristics and stress field with log data. West-China Explor. Eng. 25 (6), 467–472.

Zhang, J.B., Qin, Y., Wang, H.Y., Chen, J.G., 2003. Prediction for the occurrence of high permeability coalbed gas reservoirs with tectonics analysis. Geol. J. China Univ. 9 (3), 359–364.

Рекомендована к печати 31 мая 2017 г.
А.Э. Конторовичем

Поступила в редакцию
20 октября 2016 г.